Planetary and Space Science 129 (2016) 32–46

Contents lists available at ScienceDirect

Planetary and Space Science

journal homepage: www.elsevier.com/locate/pss

Demonstration of orbit determination for the Lunar Reconnaissance Orbiter using one-way laser ranging data

S. Bauer [a,*], H. Hussmann [a], J. Oberst [a,b,c], D. Dirkx [d,e], D. Mao [f], G.A. Neumann [g], E. Mazarico [g], M.H. Torrence [h], J.F. McGarry [g], D.E. Smith [i], M.T. Zuber [i]

[a] German Aerospace Center (DLR), Berlin, Germany
[b] TU Berlin, Germany
[c] Moscow State University for Geodesy and Cartography, Russia
[d] TU Delft, Netherlands
[e] Joint Institute for VLBI ERIC, Dwingeloo, Netherlands
[f] Sigma Space Corporation, Lanham, MD, USA
[g] NASA Goddard Space Flight Center, Greenbelt, MD, USA
[h] Stinger Ghaffarian Technologies Inc., Greenbelt, MD, USA
[i] Massachusetts Institute of Technology, Cambridge, MA, USA

ARTICLE INFO

Article history:
Received 11 February 2016
Accepted 12 June 2016
Available online 15 June 2016

Keywords:
One-way laser ranging
Orbit determination
LRO

ABSTRACT

We used one-way laser ranging data from International Laser Ranging Service (ILRS) ground stations to NASA's Lunar Reconnaissance Orbiter (LRO) for a demonstration of orbit determination.

In the one-way setup, the state of LRO and the parameters of the spacecraft and all involved ground station clocks must be estimated simultaneously. This setup introduces many correlated parameters that are resolved by using a priori constraints. Moreover the observation data coverage and errors accumulating from the dynamical and the clock modeling limit the maximum arc length.

The objective of this paper is to investigate the effect of the arc length, the dynamical and modeling accuracy and the observation data coverage on the accuracy of the results.

We analyzed multiple arcs using lengths of 2 and 7 days during a one-week period in Science Mission phase 02 (SM02, November 2010) and compared the trajectories, the post-fit measurement residuals and the estimated clock parameters. We further incorporated simultaneous passes from multiple stations within the observation data to investigate the expected improvement in positioning. The estimated trajectories were compared to the nominal LRO trajectory and the clock parameters (offset, rate and aging) to the results found in the literature.

Arcs estimated with one-way ranging data had differences of 5–30 m compared to the nominal LRO trajectory. While the estimated LRO clock rates agreed closely with the a priori constraints, the aging parameters absorbed clock modeling errors with increasing clock arc length. Because of high correlations between the different ground station clocks and due to limited clock modeling accuracy, their differences only agreed at the order of magnitude with the literature. We found that the incorporation of simultaneous passes requires improved modeling in particular to enable the expected improvement in positioning. We found that gaps in the observation data coverage over 12 h ($\approx$ 6 successive LRO orbits) prevented the successful estimation of arcs with lengths shorter or longer than 2 or 7 days with our given modeling.

1. Introduction

NASA's Lunar Reconnaissance Orbiter (LRO) was launched on June 18th, 2009 and reached its lunar orbit five days later. A comprehensive geophysical, geological and geochemical mapping of the Moon is carried out by the spacecraft in order to establish an observational framework for future lunar exploration (Zuber et al., 2010).

The Lunar Orbiting Laser Altimeter (LOLA) is one of the seven instruments onboard LRO. Its main science objectives are the derivation of a global topographic model and a high-accuracy geodetic grid. LOLA is also able to receive laser pulses from

* Corresponding author.
E-mail address: sven.bauer@dlr.de (S. Bauer).

http://dx.doi.org/10.1016/j.pss.2016.06.005
0032-0633/

Earth-based International Laser Ranging Service (ILRS) ground stations (Pearlman et al. 2002) at a single-shot precision of 15 cm. This precision is further reduced to <6 cm with an averaging of the Full Rate to Normal Point data (Bauer et al., 2016). The ranging to LRO as illustrated in Sun et al. (2013) is done from either one or multiple stations at a time. In order to receive laser shots from Earth ground stations, an optical receiver, the Laser Ranging Telescope was added to the high gain communication antenna. A fiber optic cable is forwarding incoming laser pulses into the LOLA instrument for detection. LOLA is designed so that the Earth and the Lunar return pulses can be detected concurrently with the same instrument. Further details about the ground station characteristics, the spacecraft setup including LOLA's hardware extension and the data setup can be found in Bauer et al. (2016). Both LOLA's altimetry data and the one-way range measurements provide additional observational data that complement the regular radio tracking data for orbit determination (Zuber et al., 2010; McGarry et al., 2011, 2013).

The accuracy and precision of the LRO positioning throughout the mission is critical to enable a precise referencing of the remote sensing data. From the combination of the various tracking data sets the orbit determination of LRO shall be improved in order to support Lunar precision mapping (Zuber et al., 2010).

Most of the interplanetary laser ranging experiments have been carried out only occasionally as for example to Mars Global Surveyor, MESSENGER (Neumann et al., 2006; Smith et al. 2006) and LADEE (D'Ortenzio et al., 2015). Only the ranging to LRO and the retroreflectors on the lunar surface has been done on a routine basis. While the one-way laser ranging experiment has been carried out between June 30, 2009 and September 30, 2014 (McGarry et al. 2013), two-way Lunar Laser Ranging is done since the 1970s already (Degnan, 1994). While usually one ground station is ranging to LRO at a time, other stations can join for simultaneous observations.

The LRO spacecraft is regularly tracked by NASA's radio station White Sands in New Mexico as well as by the commercial Universal Space Network (USN). From the radio tracking data the LOLA team estimates the nominal LRO trajectory via orbit determination (Mazarico et al., 2012). Within early updates of the orbit they further used LOLA's altimetric crossover data for improved solutions. Derived from the differences at the arc overlaps of trajectories consecutive in time, this nominal LRO trajectory had an overall accuracy of 23 m for the radio only and 14 m for the radio and crossover solutions (Mazarico et al., 2012). The individual arcs had a length of 2.5 days, which is typical for the orbit determination of lunar orbiters (Konopliv et al., 2001; Mazarico et al., 2010, 2012, 2013).

While using the GRAIL gravity field within the estimation, Mazarico et al. (2013) derived updated solutions that had a total average difference of ≈ 9 m at the arc overlaps over all mission phases. The GRAIL mission enabled a global estimation of the lunar gravity field to unprecedented precision from the inter-distance measurement of two co-orbiting spacecraft (Zuber et al., 2013). The most recent solutions of the nominal LRO trajectory that we use within this work incorporates the GRAIL gravity field GRGM900C (Lemoine et al., 2014) up to degree and order 600 (LRO SPICE archive, December 2015).

The application of laser ranging data for both LRO clock analysis and orbit determination was first reported by Mao et al. (2014a). Their 2-week laser-ranging-data-only arcs had differences in total of 5–30 m with respect to the nominal LRO trajectory being thus comparable in accuracy with the radio-based result. Löcher et al. (2015) and Buccino et al. (2016) also estimated orbits comparable to the radio-based results while using laser data. Except for Mao et al. (2014), the authors could not derive an improvement in positioning when using both radio and laser data within the LRO orbit determination. Since the reasons have not been reported yet, one aspect of this work is the analysis of the inherent issues of the one-way laser data application in particular.

Sun et al. (2013) and Mao et al. (2014b) reported results from simultaneous passes by multiple stations and utilized them for ground to ground time transfer with one-way data. Furthermore the positioning was expected to improve with simultaneous passes due to the geometry and the additional observations (Neumann et al., 2014). Other optical time transfer experiments like the time transfer by laser link (T2L2) and the European Laser Timing (ELT) have a two-way setup from which they derive ground to space and ground to ground time transfer (Exertier et al., 2013; Schreiber et al., 2009).

Bauer et al. (2016) characterized the LRO and the ground station clocks from single, multiple as well as simultaneous passes. They estimated the parameters offset, rate, aging and change of aging for the LRO and relative offsets and rates for the ground station clocks (ground to ground time transfer) while keeping the orbit fixed by using the nominal LRO trajectory. Within this work we also use the terms offset, rate, aging and change of aging which are equivalent to phase, frequency, frequency drift and change of frequency drift respectively as used within the time and frequency community.

This work extends the former demonstration of orbit determination based on one-way laser ranging data only by Bauer et al. (2014) from a timeframe of 5 to 7 days. Furthermore variations in the length of the trajectory and the LRO clock arc were used to research the requirements of the one-way data application within orbit determination.

In Section 2 we discuss the errors arising from the ranging measurement and the involved clocks on ground and in space. Section 3 provides a comparison of optical one- and two-way time transfer experiments and their measurement accuracy. In Section 4 we provide the theoretical background of the observation model, the estimation software with its dynamical modeling as well as the a priori constraints we apply to the state and all clocks. Further we describe the timeframe we selected for demonstration of orbit determination including the observation data coverage, characteristics of the LRO orbit, the detailed setup of the various arcs we estimated and how we analyze the estimated results. Section 5 presents our estimated trajectories with their post-fit measurement residuals, the LRO clock parameters and the ground station clock differences that we estimated and compares them to the literature. Section 6 will discuss the results and draw conclusions.

2. Measurement and clock errors

Compared to the nominal timestamp precision of 15 cm (0.5 ns) of the Full Rate LOLA data, Exertier et al. (2006) reported random errors below that within SLR. They found a 7–12 mm random error for Full Rate and 1–3 mm for Normal Point data. The errors are thereby coming from the ground station laser, detector, timer, clock and other dependencies as well as from the atmosphere and the target signature. The calibration of the station hardware, the atmosphere itself as well as the target signature introduce a systematic error of 8–19 mm.

With the ranging to LRO the LOLA time stamp accuracy is above the random error reported within SLR. With the one-way setup the systematic errors are larger than the random errors. The errors are thereby coming from the LRO onboard and the ground station clocks, the orbit that is used to complete the one-way observable as well as the modeling accuracy (see Section 4.2). Since only an uplink is used, target signature errors are not present.

The one-way observable is affected by the ground station and LRO clock stability, since their errors affect their time tags

Table 1
Stabilities of various ground station clock systems (Lombardi, 2001) and the LRO onboard clock (Cash et al., 2008).

Type	Stability @ noise floor	Averaging period τ in s
Quartz OCXO/OCCO[a]	1×10^{-12}	1 to 10^2
Rubidium	1×10^{-12}	10^3 to 10^5
Cesium/atomic	1×10^{-14}	10^5 to 10^7
H-Maser	1×10^{-15}	10^3 to 10^5
LRO USO OCXO[a]	7×10^{-14}	40

[a] Oven Controlled Crystal Oscillator.

(Dirkx, 2015a and see Eq. (7)). Table 1 shows stability values of typical ground station timing systems as well as of the LRO onboard clock.

While the ground station clocks have good stabilities over long periods (1×10^{-12} to 1×10^{-15} over 10^3 to 10^7 s), the LRO onboard clock achieves its best stability of 7×10^{-14} after an averaging period of 40 s. Overall the Ultrastable Oscillator (USO) has a stability of 1×10^{-13} between 1 and 100 s and 2×10^{-13} between 10^3 to 10^5 s at constant temperatures (Cash et al., 2008). The accumulated range error of 0.3 mm, 3 mm and 60 cm respectively becomes larger than the LOLA timestamp precision after 2500 s. Since the LRO USO stability is still at 2×10^{-13} after an orbital period of LRO of $\approx$ 120 min (7200 s) no additional once per orbit error is introduced by the onboard clock.

The response of the LRO USO rate to temperature variation is reported to be $1–3 \times 10^{-12}$/°C (Cash et al., 2008). We saw variations with an amplitude of 0.3 °C over one day that caused a maximum change in the rate of $0.3–0.9 \times 10^{-12}$ accordingly. These variations result in an accumulating offset of 13–39 ns over one day while using a sinusoidal function for the integration. This range error of $\approx$ 3–4 m over one day has an average linear trend of $1.5–4.5 \times 10^{-13}$. We observed remaining sinusoidal variations around that linear trend with an amplitude of $\approx$ 2–6 ns which. Assuming that the sinusoidal curve with a period of 1 day has a zero or a turnover point every 21,600 s, the remaining variations have an average difference in rate of $\approx \pm 1–3 \times 10^{-13}$ between these points. Since the LRO clock stability becomes larger than 2×10^{-13} after 10,000 s, the average rate difference is at or below this value. Since no correction was available for the change of rate due to temperature change within our work yet this effect influences the LRO clock approximation with polynomial fits (see Sections 5.1 and 5.2). While the periodic temperature variation mostly stays the same over the days, changes in the power consumption of nearby instruments or the orbit height can cause further changes of the temperature and thus the rate. Since the actual temperature variation is not as steady as assumed within our simplification, the periodic and further changes due to external effects mix with the stochastic noise of the clock. Because the ground station clocks are not subject to temperature change due to proper housing, their approximation is only affected by their stability.

3. Time transfer with the LRO laser ranging and other experiments

The differences between the ground station clocks which we use within the estimation and for the comparison of our parameters are derived from time transfer experiments. The two-way laser time transfer experiments T2L2 and ELT feature a similar setup consisting of a retro-reflector, a detector (providing an active uplink) and a timing system and are tracked by ILRS ground stations. The T2L2 experiment was launched onboard the Jason2 satellite in 2008 and utilizes its USO (Exertier et al., 2013). The ELT experiment will make use of the Atomic Clock Ensemble in Space (ACES) onboard the International Space Station (ISS) which will include both an atomic clock and an H-Maser (Schreiber et al., 2009). Due to the two-way setup the offset between a ground station and the onboard clock can be estimated directly (ground to space time transfer). From the offsets with respect to the onboard clock the differences between the stations are measured or remote ground station clocks are synchronized (ground to ground time transfer).

Both experiments achieve accuracies around and below 10 ps for ground to space and ground to ground time transfer. With non-common view time transfer, the ELT achieves much better accuracies than the T2L2 experiment due to the more stable clocks (Atomic and H-Maser compared to USO – see Table 1) even over one ISS orbit. With that the ELT experiment will enable global time transfer between all stations that can range to its detector.

With the one-way laser ranging we cannot derive the ground to ground time transfer from the offsets of the ground station to the onboard clock. However it is possible to measure the differences between ground station clocks directly when using the LRO clock as common reference (Bauer et al., 2016). The measured relative offsets between ground station clocks from common view LRO passes achive an accuracy of 500 ps (Sun et al., 2013).

4. Method

Fig. 1 schematically shows how the various components and steps, which will be explained in the following, are related with each other.

4.1. Time scales, clock error modeling and observation model

The theoretical description in this section closely follows the approach from Dirkx et al. (2015b) since it is employed in their estimation software which we use for the LRO orbit determination.

Depending on the velocity and the gravitational potential at the location of a clock, the rate at which local time passes varies due to relativistic effects (Einstein, 1907). We assume that a clock reads local proper time at an observer's location. We convert its times to a global timescale such as Barycentric Dynamical Time (TDB), in order to retrieve ranges that we can use within orbit determination. We use the TDB time scale since it is commonly used for ephemerides and interplanetary orbit determination.

All clocks are affected by instabilities, desynchronization, external effects and aging. We assume they register a measured proper time $\tilde{\tau}$ that differs from local proper time τ by

$$\tilde{\boldsymbol{\tau}}=\boldsymbol{\tau}+\Delta\boldsymbol{\tau}=\boldsymbol{\tau}+\Delta\boldsymbol{\tau_S}+\Delta\boldsymbol{\tau_D} \tag{1}$$

where $\Delta\tau_S$ are stochastic and $\Delta\tau_D$ deterministic errors. Our clock modeling consists of a 2nd order polynomial fit with which we estimate accumulating stochastic and deterministic errors after correcting the observation data for the influence of the atmosphere, the detector range-walk and relativistic effect on the LRO clock as reported in Bauer et al. (2016). We fit its errors via

$$\Delta\tau_{LRO}=\sum_{i=0}^{2}\Delta\tau_{LRO}^{(i)}(\tau-\tau_0)^i \tag{2}$$

where τ_0 is a reference epoch, $\Delta\tau_{LRO}^{(0)}$ the offset, $\Delta\tau_{LRO}^{(1)}$ the rate and $\Delta\tau_{LRO}^{(2)}$ the aging parameter. The errors are fitted analog for the ground station (GS) clocks 1 to n via

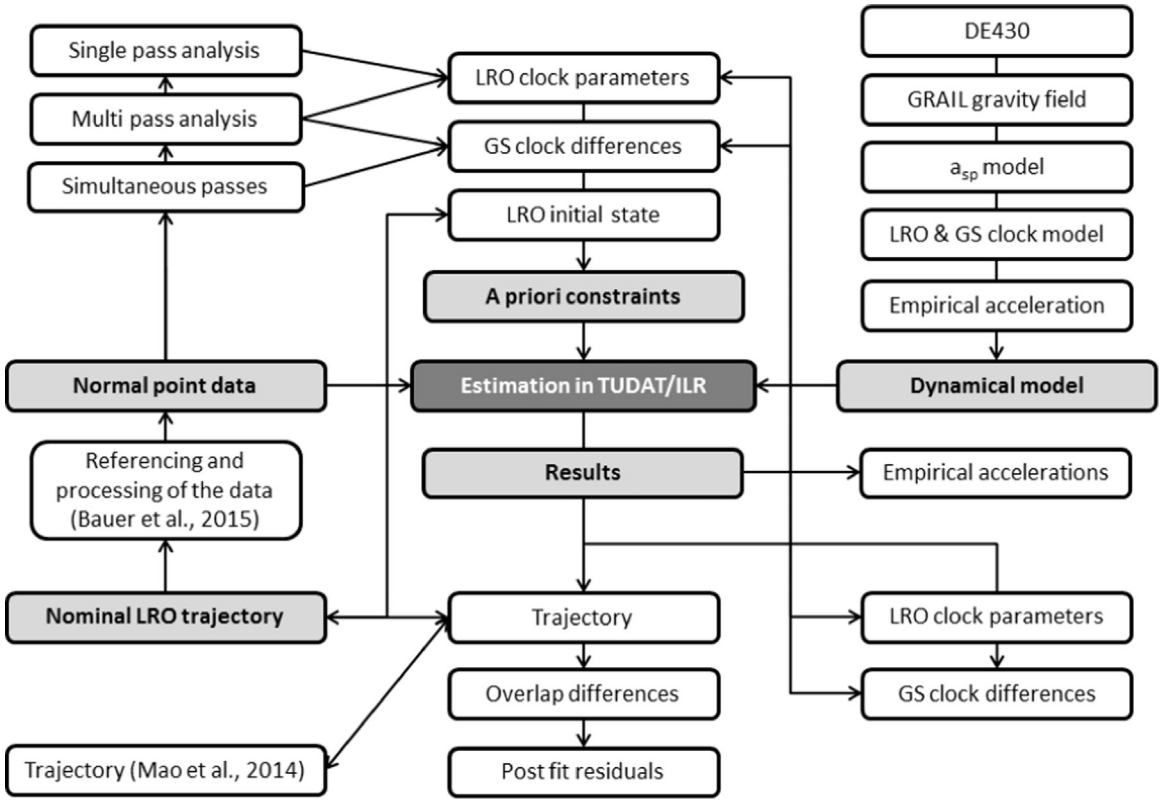

Fig. 1. Schematic overview of the relation of the various aspects of the LRO orbit determination. The gray shading highlights important major parts.

$$\Delta\tau_{GSn}=\sum_{i=0}^{2}\Delta\tau_{GSn}^{(i)}(\tau-\tau_0)^i \tag{3}$$

τ_0 is the same reference epoch as for the LRO clock, $\Delta\tau_{GS\,n}^{(0)}$ the offset, $\Delta\tau_{GS\,n}^{(1)}$ the rate and $\Delta\tau_{GS\,n}^{(2)}$ the aging parameter of the ground station clock n.

On a global timescale the one-way range $s_{LRO-GS}^{(1)}$consists of a transmission time $t_t$at the ground station and a receive time t_r at LRO

$$\boldsymbol{s}_{\boldsymbol{LRO-GS}}^{(1)}=\boldsymbol{c}\left(\boldsymbol{t_r}-\boldsymbol{t_t}\right)+\Delta\boldsymbol{s}_{\boldsymbol{LRO-GS}}^{(1)} \tag{4}$$

c is the speed of light and $\Delta s_{LRO-GS}^{(1)}$represents the range correction due to relativistic effects and the atmosphere.

The ground station and the LRO clock measure the transmission $(\tilde{\tau}_t)$ and the receive event $(\tilde{\tau}_r)$ in their proper time. Due to the one-way setup these records are separated and we first pair corresponding events with each other as described in Bauer et al. (2016). After that we retrieve the proper range from a pair via

$$\tilde{\boldsymbol{s}}_{\boldsymbol{LRO-GS}}^{(1)}=\boldsymbol{c}\left(\tilde{\boldsymbol{\tau}}_{\boldsymbol{r}}-\tilde{\boldsymbol{\tau}}_{\boldsymbol{t}}\right)+\Delta\boldsymbol{s}_{\boldsymbol{LRO-GS}}^{(1)} \tag{5}$$

By using

$$\boldsymbol{t_i}=\boldsymbol{t_i}(\tau_{\boldsymbol{i}}(\tilde{\boldsymbol{\tau}}_{\boldsymbol{i}})) \tag{6}$$

we convert measured proper time $\tilde{\tau}_i$ of a clock to true proper time τ_i and then to global time t_i. By using Eq. (5) in Eq. (6) we retrieve

$$\tilde{\boldsymbol{s}}_{\boldsymbol{LRO-GS}}^{(1)}=\boldsymbol{c}\left(\boldsymbol{t_r}-\boldsymbol{t_t}+\Delta\boldsymbol{t}_{\boldsymbol{LRO}}(\boldsymbol{t_r})-\Delta\boldsymbol{t}_{\boldsymbol{GS}}(\boldsymbol{t_t})\right)+\Delta\boldsymbol{s}_{\boldsymbol{LRO-GS}}^{(1)}+\boldsymbol{\epsilon}_{\boldsymbol{s}_{\boldsymbol{LRO-GS}}^{(1)}}, \tag{7}$$

where $\Delta t_{LRO}(t_r)$ and $\Delta t_{GS}(t_t)$ represent the time measurement error at the two clocks respectively and $\epsilon_{s_{LRO-GS}^{(1)}}$ the errors of the observed range which are independent from the clock. The latter are e.g. instrument detection accuracy, pulse length, signal strength variations and others. By using the global range from Eq. (4) we rewrite Eq. (7) as

$$\tilde{\boldsymbol{s}}_{\boldsymbol{LRO-GS}}^{(1)}=\boldsymbol{s}_{\boldsymbol{LRO-GS}}^{(1)}+\boldsymbol{c}\left(\Delta\boldsymbol{t}_{\boldsymbol{LRO}}(\boldsymbol{t_r})-\Delta\boldsymbol{t}_{\boldsymbol{GS}}(\boldsymbol{t_t})\right)+\Delta\boldsymbol{s}_{\boldsymbol{LRO-GS}}^{(1)}+\boldsymbol{\epsilon}_{\boldsymbol{s}_{\boldsymbol{LRO-GS}}^{(1)}}. \tag{8}$$

Eq. (8) shows that the measured proper range differs from the global range by the errors of the involved clocks and the errors which are independent from the clock.

Within the software the observation model for the one-way range from a ground station to LRO is implemented via

$$\boldsymbol{s}_{\boldsymbol{LRO-GS}}^{(1)}\left(\boldsymbol{t}=\boldsymbol{t_t}\right)=\left|\boldsymbol{x}_{\boldsymbol{LRO}}\left(\boldsymbol{t_t}+\frac{\boldsymbol{s}_{\boldsymbol{LRO-GS}}^{(1)}}{\boldsymbol{c}}\right)-\boldsymbol{x}_{\boldsymbol{GS}}(\boldsymbol{t_t})\right|+\Delta\boldsymbol{s}_{\boldsymbol{LRO-GS}}^{(1)}\left(\boldsymbol{t_t},\boldsymbol{t_r}\right)$$
$$+\boldsymbol{c}\left(\Delta\boldsymbol{t}_{\boldsymbol{LRO}}(\boldsymbol{t_r})-\Delta\boldsymbol{t}_{\boldsymbol{GS}}(\boldsymbol{t_t})\right). \tag{9}$$

Thereby t_t is the global transmission time at the ground station, x_{LRO} the position of LRO, x_{GS} the position of the ground station and t_r the global reception time at LRO. Since the one-way range depends on both the state and the timing of LRO, both have to be estimated from the same observable which is an inherent drawback of the one-way setup. Further the errors of the LRO and all involved ground station clocks have to be adjusted as well.

4.2. Estimation software and dynamical model

We derive the LRO orbit arcs by using a software package (Dirkx et al., 2014) that is based upon the Tudat toolbox (Kumar et al., 2012).

Because of the one-way setup we estimate the spacecraft state and the parameters of all involved clocks simultaneously (see Eqs. (8) and (9)). We estimate an initial state (position $\vec{r}_{0,LRO}$ and velocity $\vec{v}_{0,LRO}$) at a certain epoch. The orbit arcs are determined from the integration of the equations of motion from the estimated

state. Further we estimate the clock parameters offset, rate and aging for the LRO ($\Delta\tau^{(0)}_{LRO}$, $\Delta\tau^{(1)}_{LRO}$,$\Delta\tau^{(2)}_{LRO}$) and all involved ground station clocks 1 to n ($\Delta\tau^{(0)}_{GS\,n}$, $\Delta\tau^{(1)}_{GS\,n}$,$\Delta\tau^{(2)}_{GS\,n}$). For longer arcs we estimate empirical accelerations in along- and cross-track direction ($a_{emp,AT}$, $a_{emp,CT}$) to compensate for accumulating un-modeled dynamic effects.

We apply a priori initial values and covariances on the many correlated parameters that we have to estimate simultaneously (see Section 4.3). During the estimation all parameters are adjusted iteratively from their initial values within a non-linear batch least squares optimization as described by Montenbruck and Gill (2000). We use a time step of 5 s within the integration of the equations of motion.

Within the dynamical model (see Fig. 1) we used the ephemeris file DE430 (Folkner et al., 2014), in form of Spacecraft and Planetary Kernel (SPK) files for the position of the planets and the Moon.

We applied the GRAIL gravity field GGRM900C (Lemoine et al., 2014) for the representation of the lunar gravity field. We truncated the field at degree and order 180 within the estimation to reduce computation time.

We applied a “cannon-ball” model (Montenbruck, Gill, 2000) to account for the solar radiation pressure. The spacecraft is represented by a reference surface of 10m² while we assume its radiation pressure coefficient to 1.2. The spacecraft mass is changing due to the usage of fuel during maneuvers. We set it to its corresponding value during the timeframe over which we estimated the orbit. Further effects such as varying radiation pressure due to changing orientation and self-shadowing are not included. Also thermal radiation and reflected sunlight from the lunar surface are not included. Thermal radiation may cause an offset of 1–2 meters over an arc length of 2.5 days in the case of LRO (Mazarico, personal communication, 2015), i.e., 6 m over our maximal orbit arc length of 7 days. Regarding sunlight reflected from the surface we expect a total error around 9 m over 7 days for a lunar spacecraft in a 50 km circular orbit (Floberghagen et al., 1999). With both effects added to 15 m over 7 days we obtain a constant acceleration below 5×10^{-11} m/s^2 which is covered by the empirical accelerations that were estimated to values at the order of 10^{-11} m/s^2 (see Section 5.1).

Since both the state and the clocks have to be estimated with the one-way setup, errors accumulate from the imperfect modeling of the dynamics and the clock with increasing arc length. Errors of the dynamical modeling are coming from un-modeled or simplified effects within the force model such as the solar radiation pressure for example. Within the clock modeling the 2nd order polynomial fit can approximate the inherent stochastic noise of a clock only with limited accuracy (see Fig. 1 of Dirkx et al. 2015b). Furthermore the completeness and the accuracy of the corrections applied to the observation data defines how much systematics remain that have to be fitted as well. While we correct the observation data for the influence of the atmosphere, the detector range-walk and relativistic effects, the change of the LRO clock rate due to temperature change is missing. Besides the stochastic noise that is caused by the limited stability of a clock, remaining systematics have to be covered by the fits as well and affect the LRO clock approximation (see Section 2). The accumulating errors affect the estimated trajectories, their post-fit residuals and the clock parameters.

The usage of shorter clock arcs (per pass at minimum) results in more parameters that have to be estimated and leads to high correlations between the state and the clocks. Since they provide a better approximation of the stochastic clock trend, the per pass measurement post fit residuals become small. However the estimated clock parameters tend to scatter because they represent the stochastic trend during a short timescale. Furthermore they absorb signal from the state because of the correlations which also causes the trajectories to become less good.

With longer clock arcs the state and the clock become less correlated. However the errors from the dynamical modeling and the less good clock approximation are accumulating. Even though the fit represents the clock trend on average, the errors due to the stochastic noise around it increase the post-fit residuals. Furthermore the errors are absorbed by the clock parameters and let their values deviate. The trajectories also become less good since the dynamical modeling errors are accumulating, which can be absorbed by the estimation of empirical accelerations to some extent.

Overall an optimum arc length needs to be found for the state and the clocks with one-way data which provides a balance between the accuracy of the trajectory, the post-fit residuals, the clock parameters and the number of correlated parameters. The arc length thereby depends on the accuracy of the corrections, the dynamical and the clock modeling as well as the stability of the involved clocks. The optimum arc length could thereby be different for the LRO and the ground station clocks.

4.3. A priori constraints

The a priori constraints (initial values and covariances) which we use to separate and estimate the correlated state and the involved clocks are shown in Table 2.

Table 2
A priori initial and covariance values applied in the estimation.

Type	Parameter	Symbol	A priori constraints		
			Initial value	Covariance	Unit
Initial state	Position	$\vec{n}_{0,LRO}$	Taken from the nominal trajectory	$1\times10^{+06}$	m
	Velocity	$\vec{v}_{0,LRO}$		$1\times10^{+03}$	m/s
LRO clock	Offset	$\Delta\tau^{(0)}_{LRO}$	0	10	ms
	Rate	$\Delta\tau^{(1)}_{LRO}$	$-7.078e-08$	1×10^{-11}, 1×10^{-13}	–
	Aging	$\Delta\tau^{(2)}_{LRO}$	1×10^{-15} (8.6×10^{-11})	1×10^{-15} (8.6×10^{-11})	s^{-1} (day^{-1})
Ground station Clocks 1…n	Offset	$\Delta\tau^{(0)}_{GS\,n}$	0	10	ms
	Rate	$\Delta\tau^{(1)}_{GS\,n}$	0	1×10^{-11}	–
	Aging	$\Delta\tau^{(2)}_{GS\,n}$	0	1×10^{-12} (8.6×10^{-8})	s^{-1} (day^{-1})
Constant empirical accelerations	Along-track	$a_{emp,AT}$	0	1×10^{-09}	m/s^2
	Cross-track	$a_{emp,CT}$	0	1×10^{-09}	m/s^2

We use the nominal LRO trajectory to derive the initial LRO state vector at a certain epoch. We do not constraint the initial state tightly by defining large covariances. With that we check if we retrieved trajectories in agreement with the nominal trajectory after adjustment of all parameters.

Bauer et al. (2016) characterized the LRO clock from the analysis of single and multiple passes while keeping the orbit fixed. We used these parameters to define a priori initial values and covariance as described in the following.

We define the initial value of the LRO clock offset to zero, since we already applied various corrections to the one-way ranges represented by the $\Delta s^{(1)}_{LRO-GS}$ term in Eq. 4. The large covariance of 10 ms allows for the adjustment of all involved clocks simultaneously (see Eq. (8)).

The LRO clock rate has been determined accurately by Bauer et al. (2016) to a total value around 7×10^{-8} with variations slightly below 1×10^{-11} from single and multiple passes. Therefore, we define the initial value to the specific rate during the timeframe and constrain it with a covariance of 1×10^{-11}. This covariance value also is in agreement with the $3-\sigma$ variation of the single pass rates around their linear trend that we observed during the selected timeframe (see Fig. 8 in Section 5.2). Within certain arcs the rate was constrained to 1×10^{-13} in order to limit their variation due to error accumulation.

The LRO clock aging with its small value of $1.4 \times 10^{-17}\,s^{-1}$ ($1.2 \times 10^{-12}\,day^{-1}$) is especially sensitive to errors (Bauer et al., 2016). Our approximation of the LRO clock with the 2nd order polynomial fit covers stochastic clock noise less good with increasing arc length. Errors accumulate and are absorbed by the aging which is why we retrieved values at the order of $1 \times 10^{-13}\,s^{-1}$ ($8.6 \times 10^{-9}\,day^{-1}$) with long clock arcs (see Section 5.2). Tight a priori covariance constraints could mitigate the error absorption by the aging but as a result the estimated trajectories would become less good. In favor of agreement of the estimated trajectories with the nominal LRO trajectory we allow for absorption of errors and define the a priori aging covariance to $1 \times 10^{-15}\,s^{-1}$ ($8.6 \times 10^{-11}\,day^{-1}$).

As it will be seen in Section 5.3, the estimation cannot separate the ground station timing differences exactly to the measured numbers. Due to that we only define a priori covariance and no initial constraints for the offsets and the rates of the ground station clocks. The a priori offset covariance is set to 10 ms to match the LRO clock a priori offset covariance. The a priori rate covariance is set to the upper limit of 1×10^{-11} that Bauer et al. (2016) measured between the stations. The ground station clock aging covariance is constrained with $1 \times 10^{-12}\,s^{-1}$ ($8.6 \times 10^{-8}\,day^{-1}$) in order to allow for absorption of clock modeling errors as we did with the LRO clock aging.

4.4. Selected timeframe, data coverage and LRO orbit characteristics

LRO carries out various types of maneuvers at regular intervals. While yaw flips are scheduled every 6 months in order to keep the single solar panel aligned towards the sun, station keeping maneuvers were done every month and separate the overall mission into the various mission phases (commissioning – CO, nominal mission – NO01 to NO13, science mission – SM01 to SM26 and extended science mission – ES01 to ES26). In addition, desaturation maneuvers are usually carried out every two weeks to unload the reaction wheels of the spacecraft (Mazarico, 2012). The desaturation maneuvers limit the maximum free flight phase to 14 days at a time, which is the maximum possible length of orbit arcs without maneuvers. Longer arcs thereby reduce the number of correlated parameters that have to be estimated. With our modeling we found a compromise between the minimum and maximum possible arc length, the observation data coverage and the degradation of the result due to modeling errors when using a length of 2 and 7 days.

We selected a timeframe of 7 days during SM02 to demonstrate orbit determination for LRO. Fig. 2 shows the tracking data coverage during that timeframe (upper plot) and the orbit arcs we estimated (lower plot). In order to research the effect of the arc length on the results (see Section 4.2), we estimated multiple 7-day and 2-day long arcs. While the 7-day arcs Nr. 1–4 all covered the same timeframe with variations in the clock modeling, the 2-day arcs Nr. 5–10 were consecutive with overlaps of up to one day. We discuss the detailed setups of the arcs with their variations in the modeling and their tracking data coverage in Section 4.5.

We selected observational data from the three ground stations YARL, GO1L and MONL since they had the largest number of passes

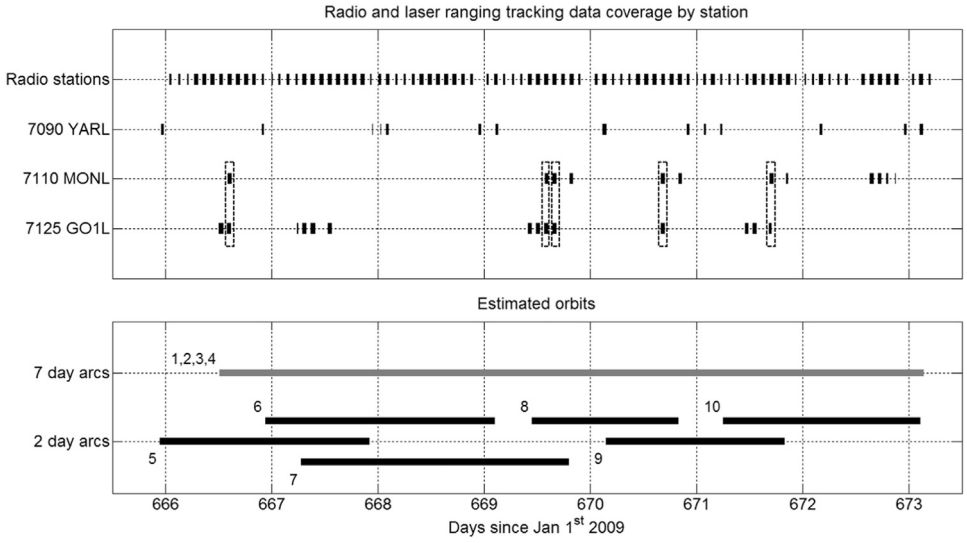

Fig. 2. The upper plot provides the coverage of LRO laser ranging data from the stations YARL, MONL and GO1L and radio (range+Doppler) data. The dashed rectangles indicate simultaneous passes. The radio passes from various stations consisting of range and Doppler measurements are added for comparison. For simplification the radio data is not grouped by type or different stations. The lower plot shows the numbered 7-day and 2-day orbit arcs that we estimated in gray and black respectively. The 7-day arcs Nr. 1 to 4 cover the same timeframe while having variations in the LRO clock arc length as well as the observation data and are thus represented by one line. The consecutive overlapping 2-day arcs are shown separately. The detailed setup will be described in Section 4.5 in detail for all orbit arcs. From the coverage of the orbits it can be seen which laser ranging passes were utilized to estimate them.

per station during the selected timeframe. We only used data from 3 ground stations in order to limit the number of correlated clocks that have to be estimated simultaneously (see Sections 4.1 and 4.2). The passes from the three stations are shown in Fig. 2 and individually listed with their characteristics in Table A.1. Table 3 lists the station coordinates, the total number of single and simultaneous passes, as well as averaged performance criteria of the stations.

The stations YARL and MONL are trailer-based Mobile Laser (MOBLAS) stations which were deployed by NASA in the 1970s in order to support the global SEASAT mission tracking (Husson, 1992). They have similar measurement characteristics due to their similar hardware (see Table 3). While their measurement precision is smaller, GO1L provides longer passes with more shots in case of the full rate data, due to the local characteristics of the laser system (higher pulse width and 28 Hz synchronized fire frequency respectively – Bauer et al., 2016).

From October 29th to November 5th 2010 there was high data coverage between the 2 US stations, with single and simultaneous passes. Even though there are no simultaneous passes between the US (GO1L and MONL) and the Australian station (YARL), the latter provides an important share of tracking data from the southern hemisphere. Thus the YARL observation data improves the observation geometry and the distribution of tracking data throughout an Earth day.

During the selected timeframe there is a laser ranging pass every 4 hours with an average length of ≈ 38 min. While the minimum time between two following passes is 134 min (consecutive orbit revolutions), there are 3 gaps longer than 12 h (see Fig. 2). While two gaps are around 12 h (12.4 h on day 666 and 12.2 h on day 670) one gap has a length of 20 h (20.4 h on day 668). While the laser ranging dataset features passes from 10 stations, these data gaps are present within this work since we only used data from 3 stations within the estimation.

For comparison Fig. 2 also shows the coverage of radio range and Doppler data from different stations. There are 88 radio passes, with an average length of 41.9 min and a maximum gap of 3.3 h during the timeframe. There are more than twice as many radio than laser ranging passes and their coverage is denser. These Doppler passes were used for the estimation of the nominal LRO trajectory (Mazarico et al., 2012).

We estimate the orbits from the laser ranging data in the Normal Point format as described in Bauer et al. (2016) with the LRO specific settings on the length and minimum number of measurements per bin (International Laser Ranging Service (ILRS), 2016). The full rate observations are grouped into bins with a length of 5 seconds starting at midnight. If there is more than one measurement per bin, they are averaged to one Normal Point. An empirical station specific range walk correction is applied to the observation data (Bauer et al., 2016).

During the selected timeframe LRO moves in an almost circular orbit with an eccentricity of $\approx 6 \times 10^{-3}$ (see Fig. 3). While LRO's orbital plane remains fixed in inertial space, its orientation relative to the observing stations changes significantly, as expressed by the angle α (see Fig. 4). Within our chosen timeframe LRO's orbital plane is initially seen "face-on" (α of 0°/180°) and finally in "edge-on" view (α of 90°/270°). While the cross-track direction is constrained well with range measurements at a "face-on" view, the along track directions have larger uncertainties in our orbit reconstruction, similar to effects observed in radio science data analysis (Mazarico et al., 2012).

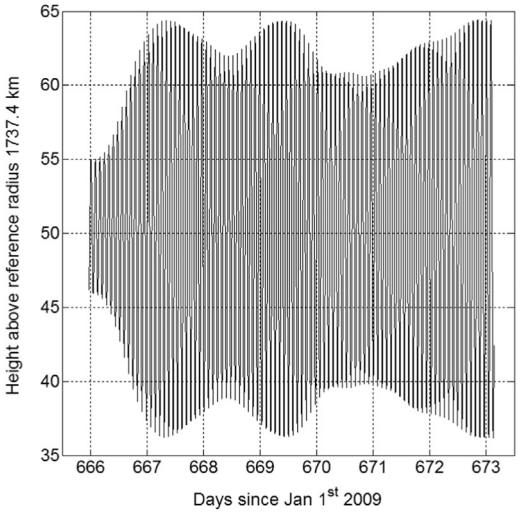

Fig. 3. Height of LRO above the surface, with reference radius of 1734.1 km (Archinal et al., 2011).

Table 3
List of the ground stations from which we used tracking data during the selected timeframe with their characteristics. Various performance criteria are listed which were averaged per station from the overall pass list in A.1. We used the observation data in the Normal Point format.

Station ID	Name	Location	Coordinates Lat.,Long.,Elev.	Timing system	Total Nr. of passes		Average[c] Pass length	Nr. of shots	Measurement precision
					Single	SP[b]	In min		In cm
7090	YARL[a]	Dongara, Western Australia, Australia	29.0464° S 115.3467° E 244 m	H-Maser	15	0	31.0	201	3.25
7110	MONL[a]	Mt. Laguna, California, USA	32.8917° N 116.4227° W 1842 m	Rubidium	7	5	36.4	210	3.69
7125	GO1L	Greenbelt, Maryland, USA	39.0206° N 76.8277° W 19 m	H-Maser	8	5	46.0	483	6.28
				Total/average value	**30**	**10**	**37.6**	**298**	**4.40**

[a] MOBLAS stations.
[b] Simultaneous passes.
[c] Normal Point data used.

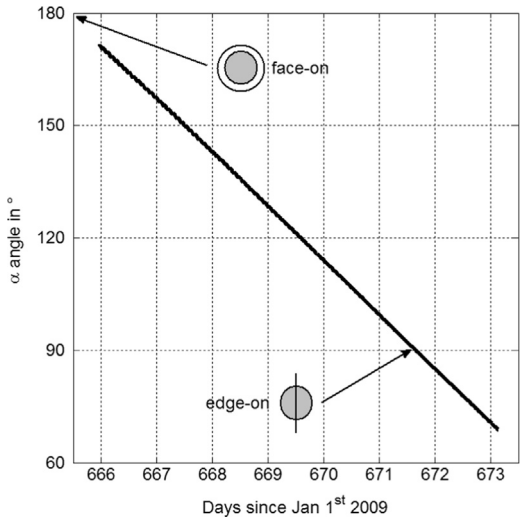

Fig. 4. α expresses the angle between the Earth – LRO vector and the orbital plane of LRO around the moon and thus an LRO orbit view-on angle from the Earth. The "face-on" and "edge-on" views from the Earth onto the orbital plane are illustrated for angles of 180° and 90°, respectively.

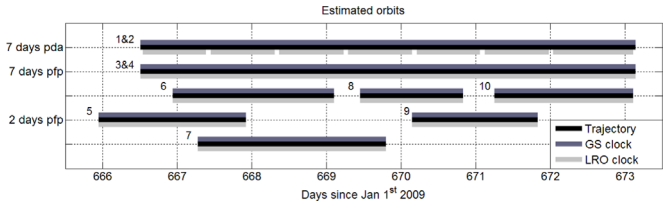

Fig. 5. Detailed setup of the estimated orbits, which consist of a trajectory, a LRO and a ground station clock arc. While the lines illustrate the length of the certain arcs – black for trajectory, dark gray for the ground station clocks and light gray for the LRO clock – the numbers label the orbits. We distinguished between orbits with a length of 7 days and 2 days, where we estimated the LRO clock either per day (pda) or per full period (pfp) over the arc. In case of the 7-day arcs Nr. 1 and 3 we further modified the observation data by adding simultaneous passes, resulting in a different trajectory but with the same coverage.

4.5. Setup of the estimated orbit arcs

Fig. 5 shows the detailed setup of the 7-day (Nr. 1 to 4) and the 2-day (Nr. 5 to 10) orbit arcs that we introduced in Fig. 2.

The arcs Nr. 1 to 4 all cover the same timeframe (day 666.51 until 673.14 since January 1st 2009). We estimated the trajectory and the ground station clocks once over the 7 days. Because we modified the LRO clock arc length and the observation data we retrieved 4 different arcs. Within arc Nr. 1 and 2 we estimated the LRO clock per day, yielding 7 clock arcs with a length of ≈ 1 day each. Within arc 3 and 4 we estimated the LRO clock once per full period, yielding 1 clock arc with a length of ≈ 7 days. In addition we introduced simultaneous passes to the observation data for both types of clock modeling (per day and per full period) to analyze how well they can be incorporated with the current modeling. Beside all single passes, we utilized one of the simultaneous passes within the arcs Nr. 1 and 3 and both within the arcs Nr. 2 and 4.

The arcs Nr. 5 to 10 have a length of ≈ 2 days which is close to the typical length used for lunar spacecraft within orbit determination (Konopliv et al., 2001; Mazarico et al., 2010, 2012, 2013). Further they are set up so that they have overlaps around one day (see Fig. 5), from which we evaluate their consistency. We estimate a trajectory and a set of LRO and ground station clock parameters over the full period of 2 days separately for every arc.

Arc Nr. 7 is longer than the others due to a 20 hours data gap on day 668 (see Fig. 2). More observation passes had to be added to enable the estimation of that arc. The other arcs have only minor variations of their length due to individual observation pass selection.

For the 7 day long arcs Nr. 1–4 we estimated empirical accelerations in order to absorb errors from un-modeled or simplified dynamic effects (see Section 4.2) that accumulate with increasing arc length. We did not incorporate simultaneous passes within the 2-day arcs because since they caused too much degradation.

4.6. Analysis of the estimated trajectories and clock parameters

As a result of a single orbit arc we obtained its trajectories, the post-fit measurement residuals, the LRO and ground station clock parameters as well as the empirical accelerations that we iterated from their a priori initial values and covariances.

We compared our estimated trajectories to the nominal LRO trajectory in the directions – along- , cross-track, radial and total for evaluation of their accuracy. Further we compared our differences to the differences of 5–30 m that Mao et al. (2014a) observed between their laser ranging data only orbits and the nominal LRO trajectory. With the 2-day arcs we further compare the differences to the nominal trajectory to the differences at the arc overlaps to evaluate their agreement.

From remaining trends of the measurement post-fit residuals we check the result precision and the modeling accuracy. Since post-fit residuals only allow for an analysis of the precision, we evaluate the trajectory accuracy from the comparison to the nominal LRO trajectory.

We compared our estimated LRO and ground station clock parameters to their a priori constraints as well as the literature. With that we check if they were estimated within their a priori constraints and how they were affected by variations of the clock arc length and clock modeling errors.

In case of the LRO clock parameters we focus on the comparison of the rate and aging. Since the offset represents a reference value and absorbs the mean clock error, as well as a mean range bias per arc it does not provide a valuable comparison.

With the ground station clocks we further compared differences in offset and rate to the corresponding differences from Bauer et al. (2016). Within this work we derived the differences for the comparison from the total offset and rate values of certain ground station combinations.

The arcs Nr. 1–10 provided us with a variety in the length of the trajectory and the clock arcs. In order to analyze the effect of the arc length on the results with the given modeling accuracy (see Section 4.2), we compare their trajectories, their post-fit residuals and their clock parameters. Furthermore we evaluate how well the simultaneous passes were incorporated with the current modeling by comparing the results of the 7-day arcs with and without them.

5. Results

In this section we present the results of the 7-day and the 2-day arcs (see Section 4.5). After evaluating the trajectories and their measurement post-fit residuals in Section 5.1, we analyze the LRO clock parameters in Section 5.2 and the ground station clock differences in Section 5.3.

5.1. Difference to the nominal LRO trajectory and post-fit measurement residuals

Table 4 lists the differences to the nominal LRO trajectory and the post-fit measurement residuals of the estimated 7-day and 2-day arcs with their specific features. In case of the 7-day arcs

Table 4
Averaged values of the 7 and the 2-day arcs with the differences with respect to the nominal LRO trajectory as well as the measurement post-fit residuals.

Arc						Other	
Nr.	Days since 2009 Jan 1st			Difference to nominal LRO trajectory	Measurement residuals	Estimation Length × number	SP included
	Begin	End	Length	m	m	–	–
1	666.51	673.14	6.63	35.11	3.69	Per day 7 × 1	No
2				42.78	4.01		Yes
3				23.79	6.76	Per full period 1 × 7	No
4				31.39	7.23		Yes
Nr.	**Days since 2009 Jan 1st**			**Difference to nominal LRO trajectory**	**Measurement residuals**	**Overlap length**	**Overlap diff**
	Begin	**End**	**Length**	**m**	**m**	**m**	**m**
5	665.97	667.95	1.98	14.63	0.37		
6	666.91	669.13	2.22	31.58	2.03	1.04	34.55
7	667.25	669.83	2.58	18.50	1.46	1.88	39.51
8	669.42	670.86	1.44	37.16	0.19	0.41	57.06
9	670.12	671.86	1.74	35.69	0.29	0.74	71.92
10	671.22	673.14	1.92	12.15	1.19	0.64	22.95
Mean			–	**24.95**	**0.92**	–	**40.61**

these are the clock modeling and the simultaneous passes. With the 2-day arcs these are the overlap lengths and differences.

Overall the differences with respect to the nominal LRO trajectory are within the reported range of 5–30 m from Mao et al. (2014a) for the best 7-day arc Nr. 3 and for the mean difference of the 2-day arcs. Increasing the arc length from 2 to 7 days increased the differences to the nominal trajectory as shown with the difference of the 7-day arc Nr. 2 compared to the mean difference of the 2-day arcs. The estimation of constant empirical accelerations once over the 7-day arcs absorbed errors from the dynamical modeling. Due to that the 7-day arc Nr. 3 achieved differences to the nominal trajectory comparable to the mean difference of the 2-day arcs (≈ 25 m).

While we estimated empirical accelerations on the order of 1×10^{-9} to 1×10^{-8} m/s^2, Mazarico et al. (2012) reported values one to two order of magnitude smaller within their LRO orbit determination. The estimation of larger empirical accelerations is caused by our less accurate dynamical modeling compared to Mazarico et al. (2012). Since the incorporation of empirical accelerations once per revolution provided no improvement while increasing the number of correlated parameters we only estimated constant empirical accelerations.

The estimation of the LRO clock per day within the 7-day arcs (Nr. 1 and 2) enabled a better approximation of its trend by the 2nd order polynomial fit. Over the shorter clock arc length less stochastic noise and variations due to temperature change have to be approximated with the fit. The accumulation of less errors allows for smaller post-fit residuals compared to the arcs where the LRO clock was estimated over the full period of 7 days (Nr. 3 and 4 – see Fig. 6). With the 2-day arcs both the state and the LRO and the ground station clocks were adjusted separately for every arc. Because of that they had even smaller post-fit residuals e.g. of only 0.19 m for arc Nr. 8 (see Table 4).

The arc overlap differences of the consecutive 2-day arcs were larger than their differences to the nominal trajectory (see Table 4). Thus the estimated trajectories were generally in agreement with the nominal trajectory even though they were scattered around it. The data gaps on day 668 (20.4 h) and on day 670 (12.2 h) that affected the arcs Nr. 7, 8 as well as 9, caused their overlaps to have large deviations in particular.

If only single passes are used from the observation data the 7-day arcs yield smaller differences to the nominal LRO trajectory and post-fit residuals for both types of clock modeling (per day and per full period). Even though it is expected that simultaneous passes should improve the solution (Neumann et al., 2014) the opposite seems to be the case – see Table 4 and Fig. 6.

The simultaneous passes were carried out by stations with different timing systems which is why they had differences in offset and rate with respect to each other. However in case of perfect dynamical and clock modeling their measurement residual differences should be close to the observation data precision (≈ 15 cm). Since the 2nd order fit that we apply over the full timeframe of 7 days cannot represent the stochastic noise of the correlated ground station clocks well enough, the measurement residual differences exceed the observation data precision at the simultaneous passes (see Sections 4.2 and 5.3). Since the passes were carried out simultaneously their approximation is not affected by the completeness and accuracy of the LRO clock corrections.

Since the simultaneous passes could not be resolved at the LOLA timestamp precision yet, more accurate dynamical and clock modeling is required in order to enable their successful application. Within the estimation we did not utilize the simultaneous passes as constraint (e.g. post-fit residuals at observation data precision) but used them as two separate single passes to benchmark our dynamical and clock modeling.

The Figs. SM.1 to SM.3 (Supplementary material) provide the differences to the nominal LRO trajectory of all arcs as well as the overlap differences of the 2-day arcs. Exemplarily the differences to the nominal trajectory of the best 7-day arc Nr. 3 and the best 2-day arc Nr. 10 are shown in Fig. 7.

The 2-day arc along- and cross-track differences to the nominal trajectory show a dependency on the alpha angle as reported by Mazarico et al. (2012) – see Fig. SM.2. At the beginning of the timeframe α is almost 180° ("face-on" – see Fig. 4) which enables a better estimation of the cross-track than the along-track elements. Accordingly the cross-track differences of the arcs Nr. 5, 6 and 7 are smaller than their along-track differences. Towards day 671.5 α becomes 90° ("edge-on"- see Fig. 4) resulting in better resolved along-track than cross-track elements as it is the case with the arcs Nr. 8, 9 and 10. This change of the along- and the cross-track accuracy with the alpha angle is also present with differences of the arc overlaps – see Fig. SM.3 for the overlaps of the arcs 5 and 6, 6 and 7 compared to the overlaps of the arcs 7 and 8, 8 and 9, 9 and 10.

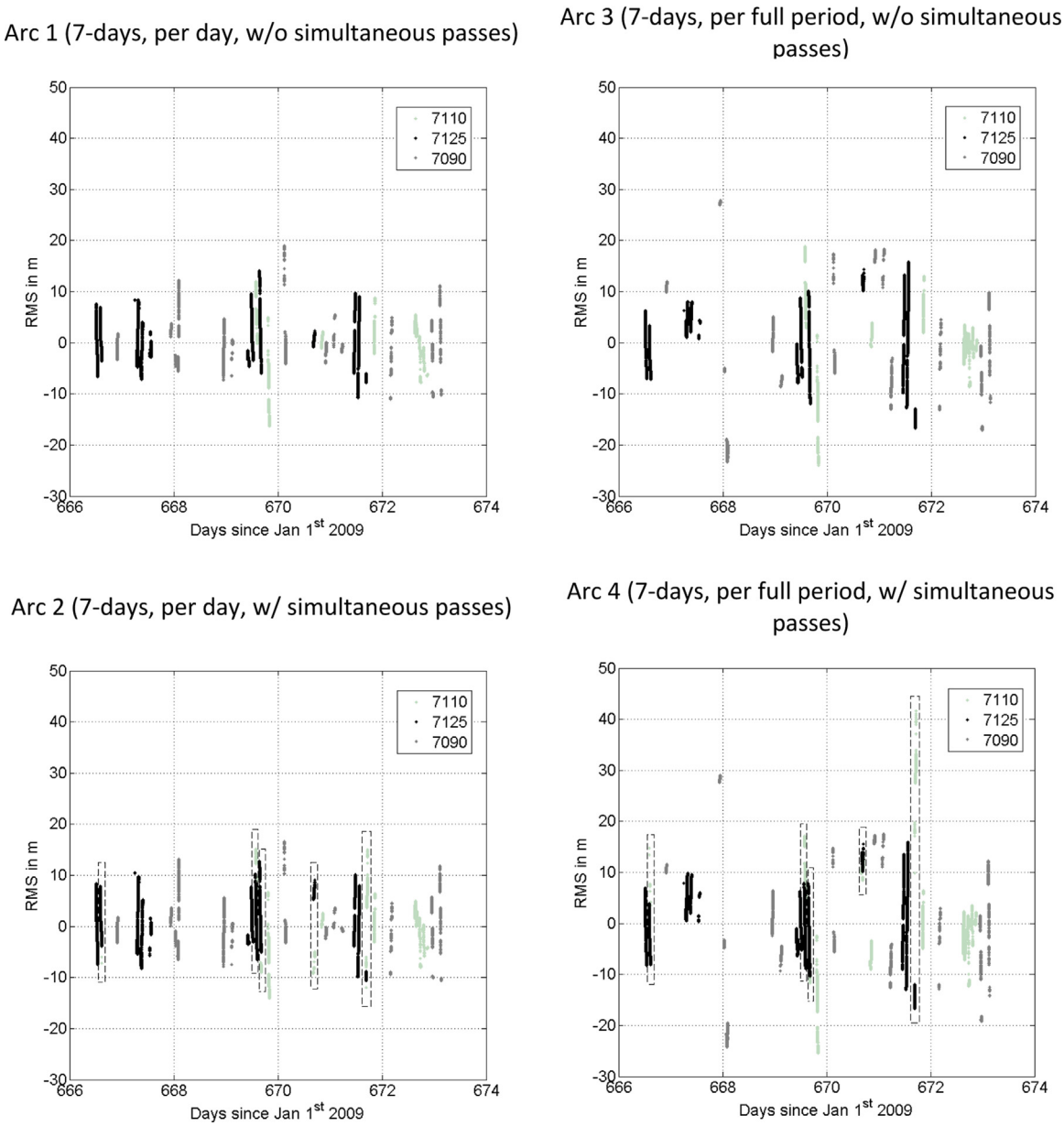

Fig. 6. Measurement post-fit residuals with respect to the estimated trajectory of the 7-day arcs 1 to 4. Arc 1 (7-days, per day, w/o simultaneous passes), Arc 2 (7-days, per day, w/ simultaneous passes), Arc 3 (7-days, per full period, w/o simultaneous passes), Arc 4 (7-days, per full period, w/ simultaneous passes).

5.2. LRO clock parameters rate and aging

Fig. 8 shows the LRO clock rate parameters $\Delta\tau^{(1)}_{LRO}$ we estimated from the applied 2nd order fit for all arcs. All estimated rate values are shown at the beginning of their state arcs respectively over which they are constant.

The rate estimated following Bauer et al. (2016) for every single or over multiple (here all plotted) passes is added. A linear fit was added to the rates of the single passes with their $3-\sigma$ error of $\approx \pm 1\times 10^{-11}$ for comparison. Neglecting the change of aging ($\approx -2.2\times 10^{-14}$ day^{-2} from Bauer et al., 2016) causes an error of $\approx 1\times 10^{-12}$ in the rate over the 7 days. Since this error is below the rate uncertainty of 1×10^{-11} this linear fit is acceptable within the comparison. The rates derived from the linear fit of single passes also were the basis for the LRO clock rate a priori constraints in Section 4.3.

While Bauer et al. (2016) used a fixed orbit (nominal trajectory) to derive the clock parameters, we adjust both the state and the clocks within this work. Due to the good accuracy of the nominal trajectory (9 m at the arc overlaps), the values derived with it provide a good comparison. Due to the fixed orbit they are affected by its state errors. However they become more accurate when estimated over multiple passes covering a longer timeframe.

While the LRO clock rates also can be estimated well from single passes, the aging of the selected timeframe ($\approx 1.6\times 10^{-12}$ day^{-1} from Bauer et al., 2016) only causes a difference of ≈ 3 cm over the average laser ranging pass length of ≈ 38 min. Since this difference is below the LOLA timestamp precision the aging value needs to be averaged over a longer timeframe with the multiple-pass analysis.

While the arcs Nr. 5–10 had an a priori covariance constraint of 1×10^{-11} on the rate, the arcs Nr. 1–4 were constrained with a covariance of 1×10^{-13} to prevent further error absorption by the parameters. With that the rates were estimated to values within the $3-\sigma$ error of the single pass rates except for the arcs Nr. 1 and 2 on day 667 and 672 within the arcs Nr. 1 and 2 as well as for arc Nr. 8 and 9. In case of the arcs Nr. 1 and 2 the outliers represent the varying LRO clock trend enabled by the shorter clock arc length of

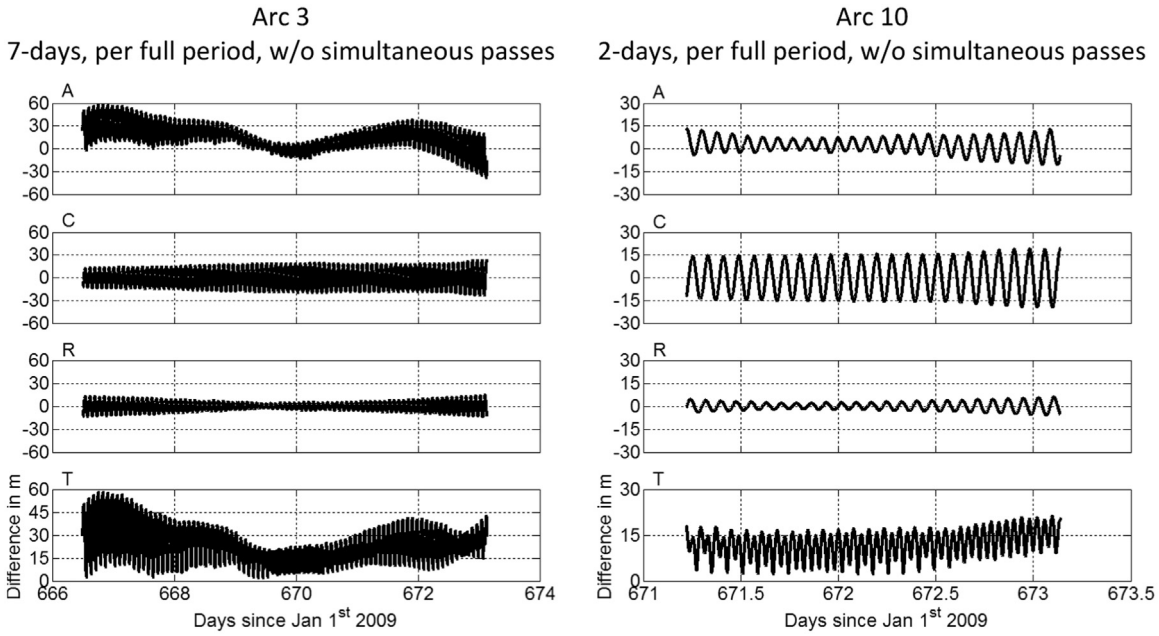

Fig. 7. Difference of the best 7-day and 2-day arc with respect to the nominal LRO trajectory in the satellite coordinate system directions along- (A), cross-track (C), radial (R) and total (T). Note the change in the scale of the time and the differences between the two arcs. Arc 3 7-days, per full period, w/o simultaneous passes, Arc 10 2-days, per full period, w/o simultaneous passes.

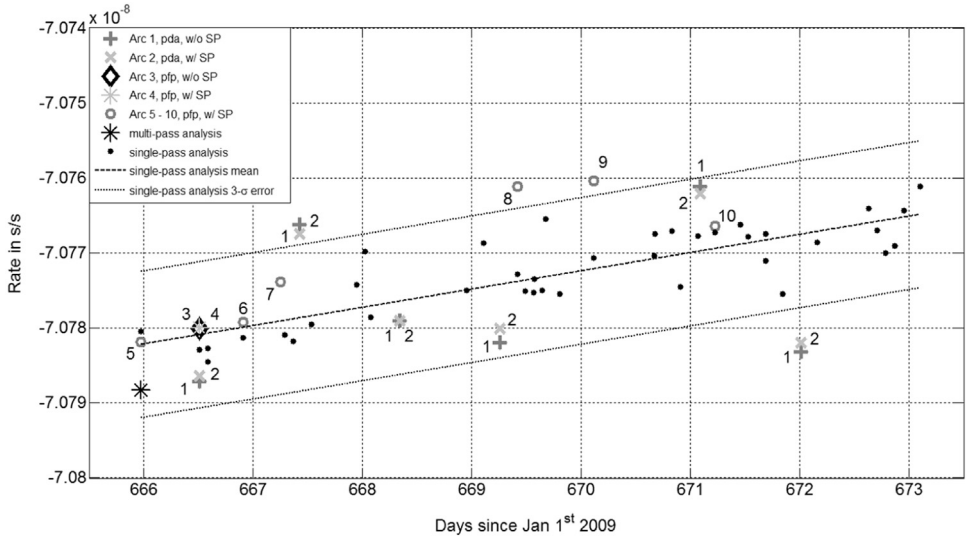

Fig. 8. Estimated LRO clock rate $\Delta\tau^{(1)}_{LRO}$ of the 7-day and 2-day arcs numbered from 1 to 10 with their variation of the LRO clock modeling (pda – per day and pfp – per full period) and the observation data (with or without simultaneous passes). For comparison the rate values from the analysis (single- and multiple-pass) based on the nominal LRO trajectory are added. For the values from the single pass analysis, the $3-\sigma$ error bounds are added.

one day (see Section 4.2). With the 2-day arcs the data gaps on day 668 and 670 that affect the arcs Nr. 7, 8 and 9 caused the estimated rates to be more off than for the arcs Nr. 5, 6 and 10. The incorporation of simultaneous passes within the 7-day arcs did not change the estimated rate significantly (see Fig. 6). Mao et al. (2011) reported a similar rate of $\approx 7\times10^{-8}$ during our selected timeframe. The rates differ by $\approx 8\times10^{-9}$ since they use UTC as time scale while we use TDB.

The LRO clock aging parameters $\Delta\tau^{(2)}_{LRO}$ we estimated from the 2nd order polynomial fit are listed in Table 5 for the 7-day arcs Nr. 1–4 and in Table 6 for the 2-day arcs Nr. 5–10. Both tables also list the values estimated with a single and multiple pass (here all plotted) analysis following Bauer et al. (2016). We applied a linear fit to the aging values of the single passes for interpolating them to the beginning of the clock arcs for a direct comparison.

The aging values estimated over 1 day (per day within the 7-day arcs) agreed best with the multiple-pass analysis value of $\approx 2.4\times10^{-12}$ day^{-1}. When estimated over 2 days we saw intermediate agreement and over 7 days (per full period within the 7-day arcs) worse agreement (see Tables 5 and 6). The incorporation of simultaneous passes within the 7-day arcs did not change the aging parameters significantly (see Table 5). While the oscillators of the New Horizons and the GRAIL mission had aging values of 1×10^{-11} day^{-1} and $7\times$10-11 day^{-1} (Weaver et al., 2004, 2010), our multiple-pass analysis and the 7-day arc per day values are in agreement with the LRO clock aging reported by Mao et al. (2011) of 3.2×10^{-12} day^{-1}.

The 2nd order polynomial is only a rough approximation of the inherently stochastic nature of the clock noise (see Fig. 1 of Dirkx et al., 2015b). Accordingly the stochastic noise and periodic

Table 5
Estimated LRO clock aging $\Delta\tau^{(2)}_{LRO}$ from the single-pass analysis, the multiple-pass analysis and the arcs where the LRO clock was estimated per full period over the 7-days (orbit arc length).

Begin date of the clock arc in days since 2009 Jan 1st	Aging $\Delta\tau^{(2)}_{LRO}$ in day^{-1}					
	Single-pass analysis	Multiple-pass analysis	Per day simultaneous passes		Per full period simultaneous passes	
			Not included Arc 1	Included Arc 2	Not Included Arc 3	Included Arc 4
666.5	$+2.1\times10^{-10}$	$+2.4\times10^{-12}$	$+2.5\times10^{-12}$	$+2.7\times10^{-12}$	-1.2×10^{-8}	-2.9×10^{-9}
667.4	$+2.4\times10^{-10}$		-2.8×10^{-11}	-2.7×10^{-11}		
668.3	$+2.7\times10^{-10}$		-4.6×10^{-12}	-4.0×10^{-12}		
669.3	$+3.0\times10^{-10}$		-2.3×10^{-12}	-4.2×10^{-12}		
670.2	$+3.4\times10^{-10}$		$+1.0\times10^{-11}$	$+1.3\times10^{-11}$		
671.1	$+3.7\times10^{-10}$		-2.1×10^{-12}	-1.8×10^{-11}		
672.0	$+4.0\times10^{-10}$		$+2.0\times10^{-12}$	$+1.8\times10^{-12}$		
Average	$\mathbf{+3.0\times10^{-10}}$	–	$\mathbf{-3.1\times10^{-12}}$	$\mathbf{-5.1\times10^{-12}}$	–	–

Table 6
Estimated LRO clock aging $\Delta\tau^{(2)}_{LRO}$ from the single-pass analysis, the multiple-pass analysis and the arcs where the LRO clock was estimated per full period over the 2-days (arc length).

Arc	Days since 2009 Jan 1st		Aging $\Delta\tau^{(2)}_{LRO}$ in day^{-1}		
Nr.	Begin	End	Single-pass analysis	Multiple-pass analysis	Per full period
5	665.97	667.95	$+1.9\times10^{-10}$	$+2.4\times10^{-12}$	$+3.7\times10^{-11}$
6	666.91	669.13	$+2.2\times10^{-10}$		-9.5×10^{-10}
7	667.25	669.83	$+2.3\times10^{-10}$		-5.8×10^{-11}
8	669.42	670.86	$+3.1\times10^{-10}$		$+7.0\times10^{-11}$
9	670.12	671.86	$+3.4\times10^{-10}$		$+7.1\times10^{-11}$
10	671.23	673.14	$+3.7\times10^{-10}$		-3.5×10^{-10}
Average			$\mathbf{+2.8\times10^{-10}}$	–	$\mathbf{-5.5\times10^{-11}}$

Table 7
Comparison of the ground station clock differences (relative offsets and rates) estimated by Bauer et al. (2016) and from the 7-day and the 2-day arcs.

	Relative offset order of magnitude	Relative rates order of magnitude
7-day arcs	10–100 ns	1×10^{-15} to 1×10^{-12}
2-day arcs	10–1000 ns	1×10^{-13} to 1×10^{-11}
Bauer et al. (2016)	1–100 ns	1×10^{-13} to 1×10^{-11}

variations due to temperature change were not captured by the fit and affected the clock parameters as well as the post fit residuals. While the LRO clock rate was mostly in agreement with it's a priori constraints even when estimated over 7 days, the aging was significantly increasing with increasing clock arc length due to error absorption – also as enabled by the a priori constraints. The increase of the post-fit measurement residuals due to accumulating clock modeling errors also can be seen in Fig. 6.

5.3. Ground station clock differences

Table 7 shows the ground station clock differences we estimated compared to the differences that Bauer et al. (2016) measured from common view time transfer during the selected timeframe. Because of the limited accuracy of the clock modeling we could not estimate the differences to the exact values from Bauer et al. (2016). However we estimated reasonable differences since at first the relative rates agree with the floor stability values of the timing systems used at the ground stations – Rubidium and H-Maser with noise floor stabilities at 1×10^{-15} to 1×10^{-12} (see Tables 1 and 3). Furthermore the differences are not larger than the upper limits measured by Bauer et al. (2016), except for the 2-day arc upper relative offset of 1000 ns. While this relative offset is too large to be realistic it highlights the absorption of clock modeling errors by the clock parameters in particular.

As shown with Eq. (7), the errors of the LRO and all involved ground station clocks have to be estimated simultaneously. The a priori constraints separate the LRO from the ground station clocks. While the errors from the ground station clocks are smaller than the LRO clock errors (similar stabilities but over longer timeframes – see Section 2), multiple stations have to be estimated with errors at the same order of magnitude. Furthermore the 2nd order polynomial fit cannot approximate the complete stochastic noise of the ground station clocks over the timeframe of 2 and 7 days. Due to the limited clock model accuracy and high correlations of all clock parameters we cannot estimate them to their actual values Furthermore the post-fit measurement residuals of the simultaneous passes were not at LOLA's observation data precision (see Fig. 7). Applying individual a priori constraints for each of the ground stations also showed no improvement, since we could not separate the highly correlated clocks with the current modeling well enough.

6. Discussion and conclusions

We used observation passes collected from ILRS ground stations to LRO for a demonstration of orbit determination with one-way laser ranging data only. We selected a timeframe of 7 days from October 28th to November 5th 2010 during the mission phase SM02.

Due to the one-way setup, the state of LRO and all involved clocks (LRO and all ground station clocks) have to be estimated simultaneously. Furthermore the errors of both the dynamical and the clock modeling accumulate with increasing arc length. The accumulation of errors thereby depends on the completeness and the accuracy of the corrections, the modeling accuracy and the stability of the involved clocks. Thus an optimum arc length is required in order to achieve a balance between the accuracy of the estimated trajectories, the measurement post-fit residuals and all clock parametersThese aspects represent inherent drawbacks of one-way data in general – compared to two-way data for example.

We used a priori constraints to separate and estimate the state

as well as all involved and correlated clocks. Our a priori constraints on the LRO initial state as well as the LRO and ground station clock parameters from Bauer et al. (2016) were derived from or while using the nominal LRO trajectory respectively. The estimated trajectories were also compared to the nominal trajectory and the clock parameters to their a priori constraints. With that we utilized a radio-based product for the analysis of laser data, the a priori constraints and as a reference for comparison of the results. However due to the good accuracy of the trajectory (9 m $\approx$ 30 ns at the arc overlaps) it provides an accurate basis and reference.

We estimated multiple 7- and 2-day long arcs within the selected timeframe. The best 7-day arc had a difference of 23.95 m to the nominal LRO trajectory and post-fit measurement residuals of 6.76 m. On average the consecutive 2-day arcs had a difference to the nominal trajectory of 24.95 m, post-fit residuals of 0.92 m and arc overlap differences of 40.91 m. The differences to the nominal trajectory were in the range that Mao et al. (2014a) observed with their 2-week long laser ranging arcs (5–30 m). The larger overlap differences of the 2-day arcs indicate that they were scattered around the nominal trajectory. Extending the state and the clock arc length from 2 to 7 days increased the difference to the nominal LRO trajectory ($\approx$ 25 m to $\approx$ 42 m) and the post-fit measurement residuals ($\approx$ 1 m to $\approx$ 7 m). The estimation of empirical accelerations within the 7-day arcs absorbed errors from the dynamical modelingand enabled the estimation of 7-day arcs with differences to the nominal trajectory comparable to the 2-day arcs ($\approx$ 25 m).

We observed a relationship between the ratio of along- and cross-track differences and the alpha angle (angle between vector Earth-LRO and normal vector of LRO's orbital plane) as observed by others during LRO orbit determination (Mazarico et al., 2012).

We estimated the LRO clock rate to values in agreement with the a priori constraints. Except for outliers due to shorter clock arc lengths and data gaps, they were within the $3-\sigma$ range ($\pm$ 1x10^{-11}) of the linear trend from the single pass rates. We estimated an average LRO clock aging value of -3.1×10^{-12} day^{-1} with a clock arc length of 1 day, of -5.5×10^{-11} day^{-1} with a length of 2 days and of 1.2×10^{-8} day^{-1} with a length of 7 days. Using methods from Bauer et al. (2016) we estimated an aging value of 2.4×10^{-12} day^{-1} during the selected timeframe. Contrary to the LRO clock rate, the aging becomes significantly larger with increasing clock arc length because the stochastic LRO clock noise and the variations due to temperature change become approximated less good by the clock model (2nd order polynomial fit).

We estimated ground station clock differences at the order of 10 to 1000 ns for the relative offset and 1×10^{-15} to 1×10^{-11} for the relative rates. Except for the outlying offset of 1000 ns the values are in agreement with the relative offsets and rates of Bauer et al. (2016). Further the relative rates agree with the noise floor stability values of the timing systems which were used at the stations. Because of the limited clock modeling accuracy, errors at similar magnitudes and high correlations between the ground station clock parameters, the differences could not be estimated to the exact values of Bauer et al. (2016). Furthermore the measurement post-fit residuals of the simultaneous passes were not at LOLA'S observation data precision.

Overall our estimation was capable of producing orbit arcs with one-way laser data only to an accuracy comparable to radio-based orbit arcs, while using less than half the number of tracking passes (40 laser compared to 88 radio passes). The incorporation of simultaneous passes did not change the estimated trajectories, the post-fit measurement residuals and the clock parameters significantly.

While the random errors observed within SLR typically limit the measurement accuracy, they are smaller than the LOLA timestamp precision with the LRO laser ranging experiment. Compared to two-way for example systematic errors are dominating with the one-way setup. They are coming from the station and the spacecraft hardware, their calibration, their timing systems and have to be modeled and estimated as well. Because all errors have to be estimated within the orbit determination simultaneously, a priori constraints are required to separate the state and all involved clocks as well as sufficient observation data coverage. Within our work we saw that gaps over 12 h degraded the result accuracy significantly in particular with arcs with a shorter length (2 days). We saw that the accuracy of the trajectories, their post-fit measurement residuals and the clock parameters became worse with increasing arc length due to errors in the modeling. Because of that an improvement of the corrections, the dynamical and the clock modeling should improve the result accuracy which should be the case with the simultaneous passes in particular.

To improve the dynamical modeling, we propose to implement a geometrical 3D spacecraft model. Such a model would allow for an improved solar radiation pressure model including effects of changing orientation of the spacecraft and self-shadowing. Additionally, indirect solar radiation pressure and thermal radiation could be incorporated. In order to improve the clock approximation, the response of the LRO clock due to thermal variation could be incorporated. If the change of the LRO clock rate can be modeled better, its approximation becomes better allowing for better residuals also over longer arc lengthsThe LRO clock approximation could further be improved by using an optimum clock arc length for the LRO and the ground station clocks. With an improved approximation, the application of a priori timing information should provide an even better separation of the involved clocks. With that less errors accumulate, which should improve the accuracy of the estimated trajectories, their post-fit residuals and the clock parameters. Moreover an improved approximation might enable the application of observation data from more than 3 stations which could close gaps in the selected observation data and further improve the result accuracy.

Finding an optimum on the state and clock arc length, that balances the trajectory, the post-fit measurement and the clock parameter accuracy would require a more extensive variation of the arc lengths. Since the observation data coverage was not coherent enough with our given modeling, arcs with further variations in the length did not provide comparable results. That has already become apparent with the adjustment of the length of arc Nr. 7 due to a $\approx$ 20 h data gap. In order to achieve results comparable to the other 2 day arcs it had to be extended to incorporate more observation data.

While a two-way laser ranging system is affected less from systematic errors than a one-way system, it requires additional and active hardware onboard the spacecraft. With a one-way ranging system the stabilities of the onboard and ground station clocks are key for the performance. While ground station clocks already provide good stabilities, onboard clocks are subject to requirements on mass and power consumption which results in a limited performance. However recent developments as the Deep Space Atomic Clock already demonstrated a stability of 1×10^{-15} day^{-1} (Ely et al., 2012) which promises better orbit determination. If multiple stations are participating in a ranging campaign, there clocks should be well referenced to a common reference such as UTC. Otherwise simultaneous passes could be used to measure their differences from common view observations. With the given stability of the DSAC, the accurate measurement of the differences also might be possible in non-common view as with the ELT experiment for example.

Overall the one-way laser ranging to LRO experiment provides a comprehensive dataset to study the capabilities and challenges of this type of tracking data. Since only minor hardware extensions on an existing instrument were required, this tracking technique is

promising for future missions that carry a laser altimeter such as the Jupiter Icy Moons Explorer (JUICE) mission from ESA.

Acknowledgments

S. Bauer, H. Hussmann, and D. Dirkx were supported by the ESPaCE project, EC FP7 Grant Agreement 263466. Major parts of this work were carried out while the first author very much enjoyed a research visit at NASA Goddard Space Flight Center (GSFC). J.O. was hosted by MIIGAiK and supported by the Russian Science Foundation, project #14-22-00197. We thank two anonymous reviewers for their very constructive comments.

Appendix A. Observation data table

See Table A1.

Table A1
List of the single and simultaneous laser ranging to LRO one-way observation passes during the 7 days timeframe with their times, length and characteristics. We used the observation data in the form of Normal Points.

Station		Pass			Average**		
ID	Name	SP*	Begin	End	Length	Nr. of Shots	Precision
			Days since 2009 Jan 1st		min		cm
7090	YARL		665.97	665.99	21.6	132	3.1
7125	GO1L		666.51	666.54	53.9	640	8.1
7125	GO1L	*	666.59	666.62	50.7	609	3.9
7110	MONL	*	666.59	666.62	46.6	31	2.4
7090	YARL		666.91	666.93	28.0	259	3.4
7125	GO1L		667.29	667.33	53.7	626	6.5
7125	GO1L		667.37	667.41	52.1	541	9.5
7125	GO1L		667.53	667.57	45.2	180	7.1
7090	YARL		667.95	667.95	08.5	94	2.6
7090	YARL		668.03	668.03	09.7	92	2.8
7090	YARL		668.08	668.10	33.8	317	3.0
7090	YARL		668.95	668.97	26.9	278	3.1
7090	YARL		669.11	669.13	35.2	202	3.2
7125	GO1L		669.42	669.45	42.1	465	4.7
7125	GO1L		669.49	669.53	53.3	600	5.4
7125	GO1L	*	669.57	669.61	53.2	632	6.4
7110	MONL	*	669.57	669.61	45.8	332	5.6
7125	GO1L	*	669.65	669.68	53.2	575	7.4
7110	MONL	*	669.67	669.68	14.8	74	2.6
7110	MONL		669.81	669.83	38.2	249	3.3
7090	YARL		670.12	670.16	53.2	255	4.1
7110	MONL	*	670.67	670.70	48.4	174	4.0
7125	GO1L	*	670.68	670.71	36.4	245	6.6
7110	MONL		670.83	670.86	44.0	329	4.1
7090	YARL		670.91	670.93	31.3	306	2.6
7090	YARL		671.07	671.09	32.2	82	4.5
7090	YARL		671.23	671.25	30.8	236	3.1
7125	GO1L		671.46	671.49	42.8	464	4.6
7125	GO1L		671.53	671.57	53.2	615	7.8
7125	GO1L	*	671.69	671.69	7.54	92	3.6
7110	MONL	*	671.69	671.73	50.4	147	3.8
7110	MONL		671.85	671.86	19.9	176	2.7
7090	YARL		672.16	672.19	38.7	114	3.4
7110	MONL		672.63	672.67	53.1	433	5.7
7110	MONL		672.71	672.74	43.7	320	3.9
7110	MONL		672.79	672.81	25.7	200	3.5
7110	MONL		672.87	672.87	05.9	55	2.7
7090	YARL		672.95	672.98	37.9	236	2.9
7090	YARL		673.11	673.14	45.8	213	3.6
7090	YARL		665.97	665.99	21.6	132	3.1
Total	**40**	**10**	**Mean**	**Value**	**37.6**	**298**	**4.4**

*Simultaneous passes.
**Normal point data used.

Appendix B. Supplementary material

Supplementary data associated with this article can be found in the online version at http://dx.doi.org/10.1016/j.pss.2016.06.005.

References

Archinal, B.A., et al., 2011. Report of the IAU working group on cartographic coordinates and rotational elements. Celest. Mech. Dyna. Astron. 109.
Bauer, S., et al., 2014. Implementation of one-way laser ranging data into LRO orbit determination. In: Proceedings of the 19th International Laser Ranging Service workshop. Annapolis, Maryland, USA, 27th–31th October.
Bauer, S., et al., 2016. Analysis of one-way laser ranging data to LRO, time transfer and clock characterization. Icarus, currently under review.
Buccino, R.D., et al., 2016. Optical Ranging measurement with a lunar orbiter: limitations and potential. J. Spacecr. Rockets.
Cash, P., et al., 2008. Ultrastable oscillators for space applications. In: Proceedings of the 40th Annual Precise Time and Time Interval (PTTI) Meeting. Reston, Virginia, USA, 1st–4th December.
D'Ortenzio, M.W., et al., 2015. Operating LADDEE: mission architecture, challenges, anomalies and success. In: Proceedings of IEEE Aerospace Conference. Big Sky, Montana, USA, 7th–14th March.
Degnan, J.J., 1994. Thirty years of laser ranging. In: Proceedings of the 9th International Laser Ranging Service workshop, Canberra, Australia, 7th–11th November.
Dirkx, D., et al., 2014. Phobos laser ranging: Numerical Geodesy experiments for Martian system science. Planet. Space Sci. 99.
Dirkx, D., 2015a. Interplanetary Laser Ranging – Analysis for Implementation in Planetary Science Missions (Ph.D. dissertation). Delft University of Technology, Delft, the Netherlands.
Dirkx, D., et al., 2015b. Comparative analysis of one- and two-way planetary laser ranging concepts. Planet. Space Sci. 117.
Einstein, A., 1907. Über das Relativitätsprinzip und die aus demselben gezogenen Folgerungen. Jahrb. Radioakt. Elektron. 4.
Ely, T.A., et al., 2012. The deep space atomic clock mission. In: Proceedings of the 23rd International Symposium on Spaceflight Dynamics. Pasadena, California, USA, 29th October–2nd November.
Exertier, P., et al., 2006. Contribution of laser ranging to Earth's sciences. C.R. Geosci. 338.
Exertier, P., et al., 2013. T2L2: five years in space. In: Proceedings of European Frequency and Time Forum & International Frequency Control Symposium (EFTF/IFC). Prague, Czech Republic.
Floberghagen, R., et al., 1999. Lunar albedo force modeling and its effect on low lunar orbit and gravity field determination. Advances in Space Research 23 (4).
Folkner, W.M., et al., 2014. The planetary and lunar ephemerides DE430 and DE431. IPN Prog. Rep., 42–196.
Husson, V.S., 1992. Historical MOBLAS system characterization. In: Proceedings of the 8th International Laser Ranging Service workshop. Annapolis, Maryland, USA, 18th–22th May.
International Laser Ranging Service (ILRS) Website. ⟨http://ilrs.gsfc.nasa.gov⟩ retrieved in April 2016.
Lemoine, F., et al., 2014. GRGM900C: a degree 900 lunar gravity model from GRAIL primary and extended mission data. Geophys. Res. Lett. 41 (10).
Lombardi, M.A., 2001. Fundamentals of Time and Frequency, published in The Mechatronics Handbook. CRC Press.
Konopliv, A.S., et al., 2001. Recent gravity models as a result of the lunar prospector mission. Icarus 150.
Kumar, K., et al., 2012. TUDAT: a modular and robust astrodynamics toolbox. In: Proceedings of the 5th International Conference on Astrodynamic Tools and Techniques (ICATT), ESTEC/ESA. The Netherlands, 29th May–1st June.
Löcher, A., et al., 2015. Towards improved lunar reference frames: LRO orbit determination. In: Proceedings of International Association of Geodesy Symposia. Springer.
Mao, D., et al., 2011. Laser ranging experiment on Lunar Reconnaissance Orbiter: timing determination and orbit constraints. In: Proceedings of the 17th International Workshop on Laser Ranging. 16–20 May 2011. Bad Kötzting, Germany.
Mao, D., et al., 2014a, LRO orbit determination with laser ranging data. In: Proceedings of the 19th International Laser Ranging Service Workshop Annapolis. Maryland, USA, 27th–31th October.
Mao, D., et al., 2014b. Time-transfer experiments between satellite laser ranging ground stations via one-way laser ranging to the Lunar Reconnaissance Orbiter. In: Proceedings of the 19th International Laser Ranging Service Workshop. Annapolis, Maryland, USA, 27th–31th October.
Mazarico, E., et al., 2010. GLGM-3: a degree-150 lunar gravity model from the historical tracking data of NASA Moon orbiters, JGR, 115.
Mazarico, E., et al., 2012. Orbit determination of the Lunar Reconnaissance Orbiter. J. Geod. 86.
Mazarico, E., et al., 2013. Improved orbit determination of lunar orbiters with lunar gravity fields obtained by the GRAIL mission. In: Proceedings of the 44th Lunar and Planetary Science Conference (LPSC). Woodlands, Texas, USA, 18th–23rd March.
McGarry, J., et al., 2011. The first ILRS laser transponder mission: laser ranging to

NASA's Lunar Reconnaissance Orbiter. In: Proceedings of the 17th International Laser Ranging Workshop. Bad Koetzting Germany, 16th–20th May.
McGarry, J., et al., 2013. LRO-LR: four years of history-making laser ranging. In: Proceedings of the 18th International Laser Ranging Workshop. Fujiyoshida Japan, 11th–15th November.
Montenbruck, O., Gill, E., 2000. Satellite Orbits. Springer, Berlin, London.
Neumann, G.A., et al., 2006. Laser ranging at interplanetary distances. In: Proceedings of the 15th International Laser Ranging Workshop. Canberra, Australia, 15th–20th October.
Neumann, G.A., et al., 2014. Interplanetary laser ranging: the quest for 1 AU. In: Proceeding of the 19th International Laser Ranging Service Workshop. Annapolis, Maryland, USA, 27th–31th October.
Pearlman, M.R., et al., 2002. The international laser ranging service. Adv. Space Res. 30 (2).
Schreiber, U., et al., 2009. The European Laser Timing (ELT) experiment on-board ACES. In: Proceedings of the 23rd European Frequency and Time Forum (EFTF 2009). Neuchâtel, Switzerland.
Smith, D.E., et al., 2006. Two-Way laser link over interplanetary distance. Science 311 (53).
Sun, X., et al., 2013. Free space laser communication experiments from Earth to the Lunar Reconnaissance Orbiter in lunar orbit. Opt. Express 21 (2).
Weaver, G., et al., 2004. Developments in ultra-stable quartz oscillators for deep space reliability. In: Proceedings of the 36th Annual Precise Time and Time Interval (PTTI) Systems and Applications Meeting. Washington, DC, USA, 7th–9th December.
Weaver, G., et al., 2010. The Performance of Ultra-Stable Oscillators for the Gravity Recovery and Interior Laboratory (Grail). In: Proceedings of the 42nd Annual Precise Time and Time Interval (PTTI) Systems and Applications Meeting. Reston, Virginia, USA, 15th–18th November.
Zuber, M.T., et al., 2010. The Lunar Reconnaissance Orbiter laser ranging investigation. Space Sci. Rev. 150.